

## Fabrication and Characterization of novel $W_{80}Ni_{10}Nb_{10}$ alloy produced by mechanical alloying

R. Saxena, A. Patra<sup>1</sup>, S. K. Karak, A. Pattanaik, S. C. Mishra

Department of Metallurgical and Materials Engineering, National Institute of Technology, Rourkela-769008, Orissa, India

Corresponding author Email : patraa@nitrkl.ac.in/anspat.met@gmail.com

**Abstract:** Nanostructured tungsten (W) based alloy with nominal composition of  $W_{80}Ni_{10}Nb_{10}$  (in wt. %) was synthesized by mechanical alloying of elemental powders of tungsten (W), nickel (Ni), niobium (Nb) in a high energy planetary ball-mill for 20 h using chrome steel as grinding media and toluene as process control agent followed by compaction at 500 MPa pressure for 5 mins and sintering at 1500°C for 2 h in Ar atmosphere. The phase evolution and the microstructure of the milled powder and consolidated product were investigated by X-ray diffraction (XRD), Scanning electron microscopy (SEM) and Transmission electron microscopy (TEM). The crystallite size of W in  $W_{80}Ni_{10}Nb_{10}$  powder was reduced from 100  $\mu\text{m}$  at 0 h to 45.6 nm at 10 h and 34.1 nm at 20 h of milling whereas lattice strain increases to 0.35% at 20 h of milling. The dislocation density shows sharp increase up to 5 h of milling and the rate of increase drops beyond 5 to 20 h of milling. The lattice parameter of tungsten in  $W_{80}Ni_{10}Nb_{10}$  expanded upto 0.04% at 10 h of milling and contracted upto 0.02% at 20 h of milling. The SEM micrograph revealed the presence of spherical and elongated particles in  $W_{80}Ni_{10}Nb_{10}$  powders at 20 h of milling. The particle size decreases from 100  $\mu\text{m}$  to 2  $\mu\text{m}$  with an increase in the milling time from 0 to 20 hours. The crystallite size of W in milled  $W_{80}Ni_{10}Nb_{10}$  alloy as evident from bright field TEM image was in well agreement with the measured crystallite size from XRD. Structure of W in 20 h milled  $W_{80}Ni_{10}Nb_{10}$  alloy was identified by indexing of selected area diffraction (SAD) pattern. Formation of NbNi intermetallic was evident from XRD pattern and SEM micrograph of sintered alloy. Maximum sinterability of 90.8% was achieved in 20 h milled sintered alloy. Hardness and wear study was also conducted to investigate the mechanical behaviour of the sintered product. Hardness of  $W_{80}Ni_{10}Nb_{10}$  alloy reduces with increasing load whereas wear rate increases with increasing load. The evaluated hardness value in the present study for all loads is lower than the literature reported hardness of nanostructured W.

### 1. Introduction

Tungsten is a candidate material for electrical, electronic, nuclear and space vehicle application owing to highest melting point (3410°C) and density (19.3 g/ml) of all engineering materials, excellent mechanical strength at elevated temperature, and tensile elastic modulus of 411 GPa. [1]. However poor fabricability and high ductile-brittle transition temperature of tungsten limited the wide range of application. In order to improve the properties and to increase the spectrum of applicability, much effort has been directed towards the development of tungsten alloys in recent years. The work is

<sup>1</sup> patraa@nitrkl.ac.in/anspat.met@gmail.com (Prof. A. Patra)



essentially centered on the goals such as to improve fabricability, particularly at elevated temperatures and to lower the ductile brittle transition temperature of W based alloys. As a result of increasing demand for higher and better mechanical properties, amorphous and nanocrystalline tungsten alloys have attracted enormous attention in recent years [2, 3]. Mechanical properties of nanostructured materials are known to be improved by the refinement of microstructures by mechanical alloying which is a convenient solid state synthesis method alternative to melt spinning and similar rapid quenching techniques to develop crystalline and amorphous alloys [4]. Among the various solid state methods, high-energy ball milling has gained quite popularity in recent years because of its simplicity, ease scale up production, high productivity, relatively inexpensive equipment, and applicability to a wide variety of materials [5]. Addition of nickel facilitates liquid phase sintering if sintering is carried out at a temperature higher than the melting point of Nickel (1455°C) whereas Nb addition improves high temperature response of W [1].

Present investigation aims at lowering the sintering temperature of  $W_{80}Ni_{10}Nb_{10}$  alloy by formation of nanostructure by mechanical alloying prior to sintering. Characterization of milled and consolidated  $W_{80}Ni_{10}Nb_{10}$  alloy was also carried out.

## 2. Materials and methods

A planetary ball mill (Fritsch Pulverisette P5) was used to mill elemental W, Ni, Nb powder at a mill speed of 300 r.p.m using chrome steel as grinding media and ball to powder weight ratio of 10:1. Milled samples were taken out after 1, 5, 10, 15, 20 h for characterization purpose. The details of the selected alloy and milling parameters are presented in the table 1.

**Table 1.** Details of alloy composition and milling parameters

Composition (wt.%)	Grinding Medium	Ball to powder weight ratio	Mill Speed (rpm)	Milling Duration (h)	Milling Medium
$W_{80}Ni_{10}Nb_{10}$	Chrome Steel	10:1	300	20	Toluene

A high resolution X-ray diffractometer (Make: Rigaku Japan, Model: Ultima IV) was employed to record the X-ray diffraction pattern (XRD) of the mechanically alloyed powders at different stages of milling as well the sintered alloy using Cu- $\alpha$  radiation ( $\lambda=1.541874 \text{ \AA}$ ). Evolution of phases during mechanical alloying was detected by matching the XRD results with JCPDS data bank [6]. Measurement of the crystallite size and lattice strain was carried out by evaluation of the peak position and broadening of peak from the X-ray diffraction pattern [7].

Dislocation density of the milled powder was calculated from the equation below:

$$\rho_d = 2\sqrt{3} \frac{(\varepsilon^2)^{1/2}}{D X b} \quad (1)$$

Where, b is the burgers vector of dislocations,  $b = (a\sqrt{3})/2$  for the bcc structure, a= cell parameter = lattice parameter, D = crystallite size,  $\varepsilon$  = lattice strain, [8].

The lattice parameter was measured from the X-ray diffraction pattern by stripping of  $K\alpha_2$  of XRD pattern using precise lattice parameter calculation method [7]. The precise measurement of d at  $\cos(\theta)$  tending to 0 was carried out by extrapolating the d values of the high angle diffraction peaks against the function  $\cos^2(\theta)/\sin(\theta)$ ,  $\cos^2(\theta)$  [6]. It was evident that  $\cos^2(\theta)$  function displayed the best possible fit. Scanning electron microscope (SEM) (Make: JEOL, Model: JSM-6084LV) was used to investigate the morphology of the mechanically alloyed (MA) powders at different periods of milling

and the microstructure of the sintered product. A test tube containing the 20 h milled powder was dissolved in acetone and placed in an ultrasonic vibrator for vigorous stirring. The powder was positioned on a carbon grid before TEM study. Detection of crystallite size of nanostructured W in mechanically alloyed  $W_{80}Ni_{10}Nb_{10}$  powder at 20 h of milling was carried out by transmission electron microscope (TEM) (Make : JEOL, Japan, Model- JEM 2100). Crystal structure was identified by selected area diffraction (SAD) pattern using appropriate aperture and tilt. The 20 h milled powders were subjected to compaction in a uniaxial press at 500 MPa pressure for 5 mins followed by sintering at 1500°C for 2 h with Argon purging at the rate of 100 ml/min. Microhardness of the sintered product was evaluated by a Microhardness tester (Make: Leco, Model: LM248AT) with varying load of 50 gf, 100 gf, 500 gf, 1000 gf for 10 sec. A ball on plate wear tester (Make: Ducom, Model: TR-208-M1) was employed to determine the wear depth with sliding distance of the indenter on the sintered sample with 20 N and 30 N load. The sliding speed and time was kept at 25 r.p.m and 10 mins respectively.

### 3. Result and Discussion

#### 3.1. X-ray Diffraction (XRD) analysis of milled powder

Figure 1 shows the XRD patterns of as milled  $W_{80}Ni_{10}Nb_{10}$  powder at different milling times (1, 5, 10, 15, 20 h). Refinement of crystallite size of W with increase in milling time is due to continuous broadening and reduction in the intensity of the XRD peaks. Formation of solid solution (Ni and Nb undergoes into W matrix) with increase in milling time is evident from figure 1. Decrease in crystallite size and increase in plastic strain is due to the increase in full-width at half-maximum with increasing milling time [9]. Scherrer equation was used to analyse the peak broadening after removing the strain and instrumental error components [6].

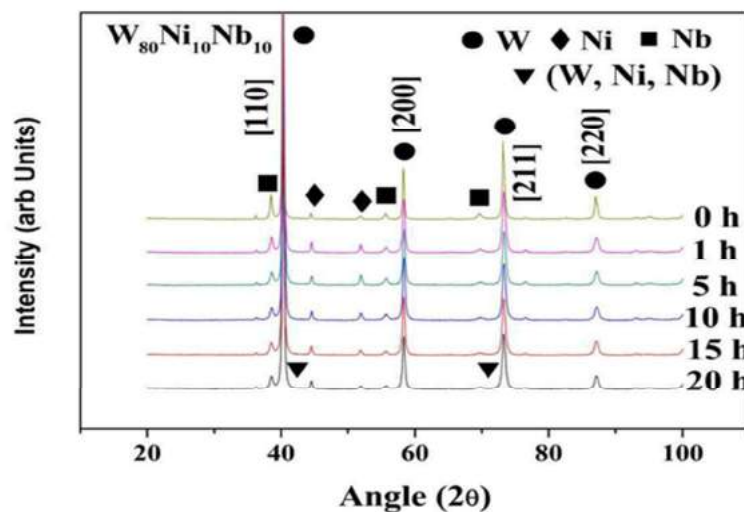


Figure 1. XRD pattern of  $W_{80}Ni_{10}Nb_{10}$  alloy milled for 20 h.

The crystallite size and lattice strain was calculated by using Williamson–Hall equation [10] as:

$$\beta \cos \theta = \frac{0.94\lambda}{D} + 4\eta \sin \theta \quad (2)$$

where,  $\beta$  is the full width half maxima (FWHM),  $D$  is the crystallite size and  $\eta$  is the lattice strain.

Figure 2 displays the variation of crystallite size and lattice strain with milling time. The crystallite size is 34 nm at 20 h of milling for  $W_{80}Ni_{10}Nb_{10}$  composition. Recent literature suggest that the crystallite size of W based alloys can be reduced more (30 nm) than the present study at 20 h of milling using

tungsten carbide (WC) grinding media during milling [1]. Tungsten carbide possess higher hardness as compared to chrome steel resulted in more reduction in crystallite size [1].

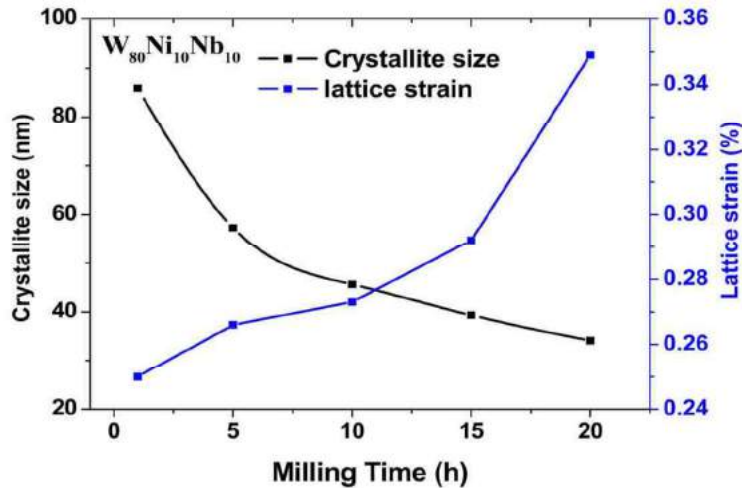


**Figure 2.** Variation of crystallite size and lattice strain of W with milling time in  $W_{80}Ni_{10}Nb_{10}$ .

Figure 3 (a) illustrates that dislocation density induced in  $W_{80}Ni_{10}Nb_{10}$  alloy increases sharply at 5 h of milling, however moderate increase is evident beyond 10 h of milling. Expansion of lattice parameter of W upto 0.04% at 10 h and contraction upto 0.02 % beyond 10 to 20 h of milling is evident from figure 3 (b). Recent report suggests that exertion of negative hydrostatic pressure due to the formation of nano-crystallites during mechanical alloying of pure Nb resulted in significant expansion of Nb lattice [11]. The present investigation also displays a similar trend. Nb and Ni form substitutional solid solution with W matrix. The atomic radius of W (0.193 nm) is larger than Ni (0.149 nm) and smaller than Nb (0.198 nm). Therefore the resultant atomic radius shows a decrease beyond 10 h of milling [12]. Predominant reduction in crystallite size at 10 h of milling is responsible for sharp increase in dislocation density whereas formation of solid solution (alloying of Nb and Ni with W) dominates over crystallite size reduction beyond 10 to 20 h of milling which results in marginal increase in dislocation density and decrease in lattice parameter. However the decrease in lattice parameter in the present study is lower than recent investigation on mechanically alloyed  $W_{80}Ni_{10}Mo_{10}$  as atomic radius of both Ni (0.149 nm) and Mo (0.190 nm) is lower as compared to the atomic radius of W [13].

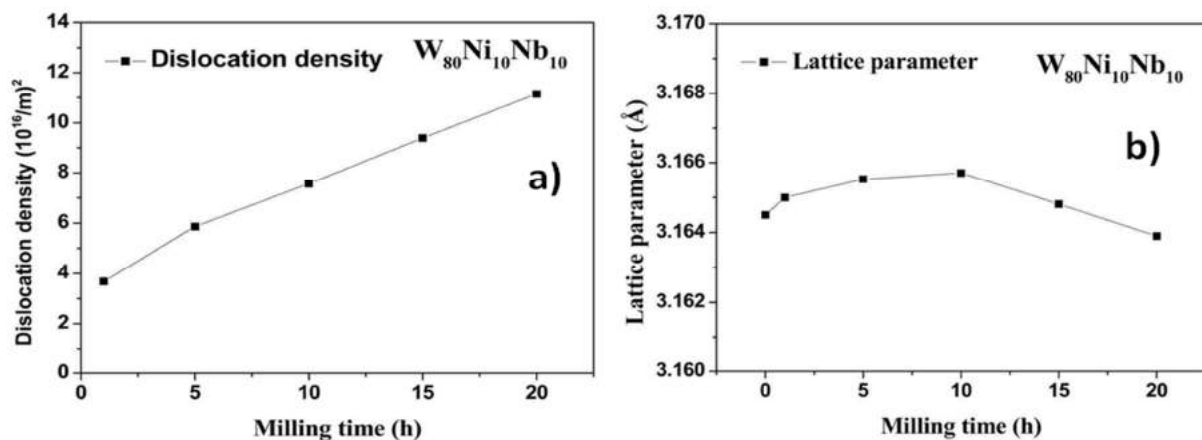


**Figure 3.** Variation of a) Dislocation density and b) Lattice parameter of W in  $W_{80}Ni_{10}Nb_{10}$  with milling time.

### 3.2. Scanning Electron Microscope (SEM) analysis of milled powder

Figure 4 (a-d) displays the variation of particle morphology and size of the milled powder at different milling time. The particle size changes from  $\sim 100\ \mu\text{m}$  to  $\sim 2\ \mu\text{m}$  with increase in milling time. The particles are continuously strain hardened and fractured with increase in milling time. The spherical shape of W, Ni and Nb particles at 0 h change to elongated shape at 20 h of milling. Welding of some particles is also evident at 10 h of milling (figure (4c)). The elongated nanoparticles at 20 h of milling results in poor flowability due to large interparticle friction therefore responsible for poor green densification property [13].

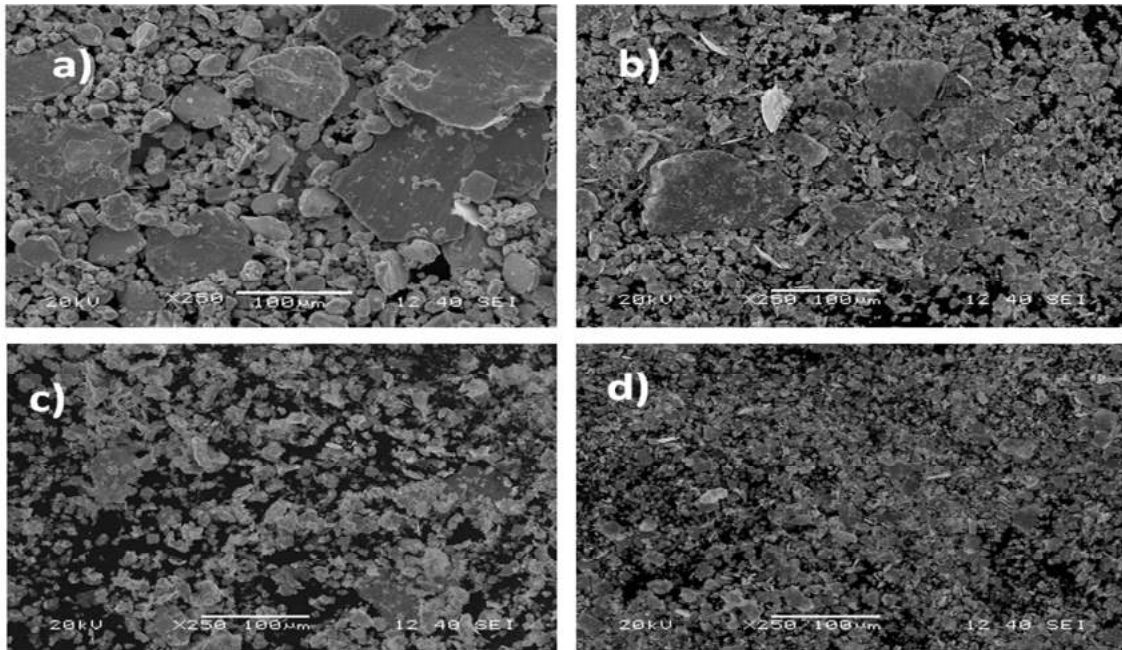


**Figure 4.** SEM images of powder morphology of  $\text{W}_{80}\text{Ni}_{10}\text{Nb}_{10}$  alloy after different milling times: (a) 0 h, (b) 5 h, (c) 10 h, and (d) 20 h.

### 3.3. Transmission Electron Microscope (TEM) analysis of milled powder

Figure 5 (a) and (b) displays bright field TEM image along with corresponding SAD pattern of  $\text{W}_{80}\text{Ni}_{10}\text{Nb}_{10}$  powder milled for 20 h. Formation of nano-crystallites at 20 h of milling with size varying from 20 to 30 nm is evident from figure 5(a). The observed crystallite size nearly matches with the crystallite size derived from XRD analysis (figure 2). Continuous rings evident from SAD pattern confirm the presence of fine polycrystallites. Indexing of SAD pattern shows the presence of (110), (200), (222) planes of W. The measured interplaner spacing (d) values of BCC-W are 0.22 nm for (110), 0.15 nm for (200), and 0.09 nm for (222) respectively. The interplaner spacing (d) values matches well with the standard values of BCC-W from JCPDS data files.

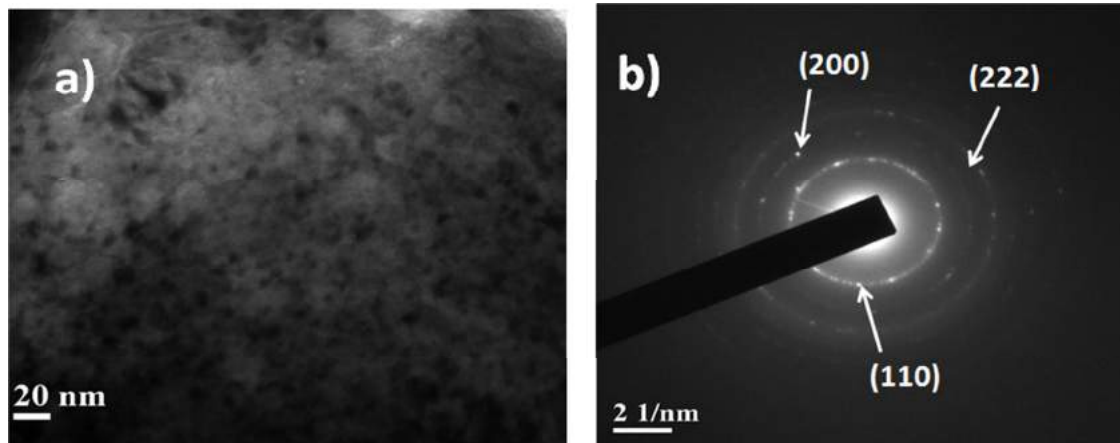


**Figure 5.** TEM image of  $W_{80}Ni_{10}Nb_{10}$  powder milled at 20 h: (a) Bright field TEM image and (b) corresponding SAD pattern.

#### 3.4. X-ray Diffraction (XRD) analysis of sintered alloy

Figure 6 displays the XRD pattern of sintered  $W_{80}Ni_{10}Nb_{10}$  alloy. Formation of brittle hard intermetallic NbNi is evident from the XRD pattern. The strength of the W matrix could be enhanced by the presence of NbNi intermetallic. Formation of NbNi intermetallic is also reported by Li et al. [14]. Any unwanted phase transition apart from formation of NbNi intermetallic is not evident from the XRD pattern.

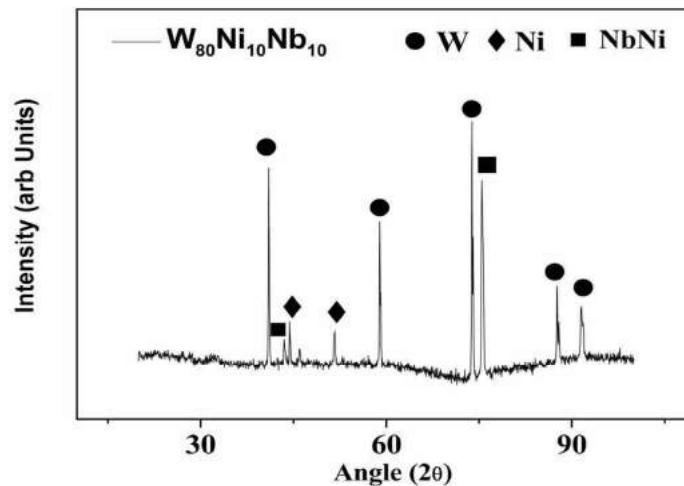


**Figure 6.** XRD pattern of  $W_{80}Ni_{10}Nb_{10}$  alloy milled for 20 h and sintered at 1500°C for 2 h.

#### 3.5. Scanning Electron Microscope (SEM) analysis of sintered alloy

Figure 7 displays the SEM micrograph of  $W_{80}Ni_{10}Nb_{10}$  alloy sintered at 1500°C for 2 h. The micrograph reveals the presence of dark phase (Ni) in W matrix (bright phase). The formation of NbNi intermetallic phase as evident from figure 7 is due to the lower melting point of Ni (1455°C) as compared to the sintering temperature (1500°C) selected for the present investigation. The phases evident from SEM micrograph match well with the identified phases from the XRD analysis.

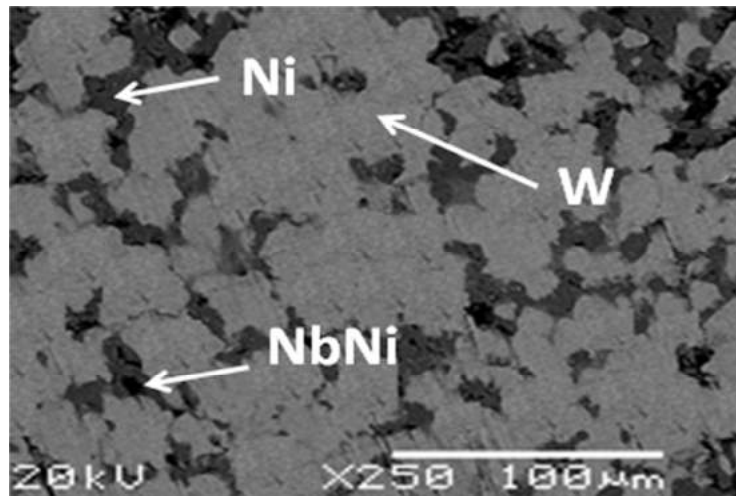


**Figure 7.** SEM micrograph of 20 h milled  $W_{80}Ni_{10}Nb_{10}$  alloy sintered at 1500°C for 2 h.

### 3.6. Sinterability study

Sinterability is defined as the percentage ratio of sintered sample density to theoretical density of the sintered sample. Sintered alloy density can be calculated by Archimedes' principle [15] as below:

$$\rho_s = \frac{W_a}{(W_{sat} - W_{susp})} \times \rho_w \frac{\text{gm}}{\text{cm}^3} \quad (3)$$

Where  $W_a$  is weight of the sintered sample in air.  $W_{sat}$  is the weight of the sample with all the open porosity saturated with water,  $W_{susp}$  is the weight suspended in water.  $\rho_w$  is the density of water. The sinterability of the 20 h milled sample sintered at 1500°C for 2 h is recorded 90.8% by pressing at 500 MPa pressure for 5 mins.

### 3.7. Hardness study

The microhardness can be measured by using the equation as [16]:

$$HV = 1.8544 \frac{P}{d^2} \quad (4)$$

where P is the applied load and d is the diagonal length of the indentation.

Figure 8 shows the variation in hardness along the cross section of the  $W_{80}Ni_{10}Nb_{10}$  alloy with varying load. It is evident from the figure that hardness increases with decrease in applied load. This is attributed to appreciable elastic recovery at lower load and error in appropriate detection of diagonal length of the indentation due to smaller indentation at lower loads [17]. The variation in hardness for a specific load at different point of the sample may be due to variation in composition through the cross section. The average hardness for all loads is lower than recently investigated nanostructured W due to softening of W lattice by addition of Ni and Nb [1].

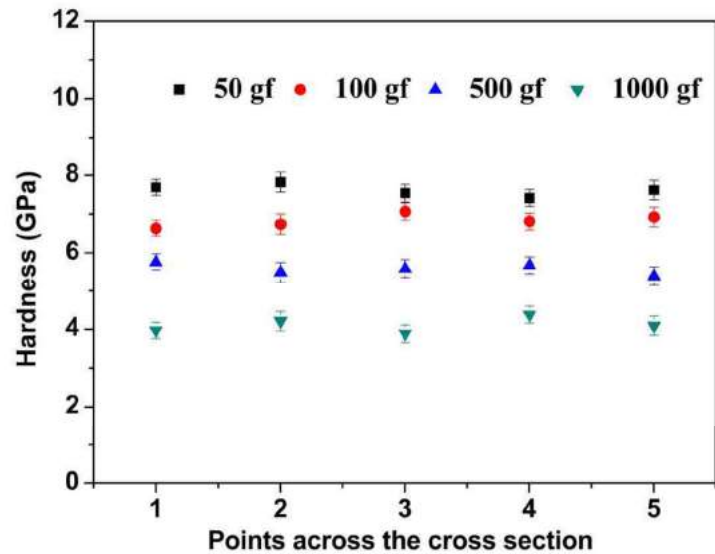


**Figure 8.** Variation of Hardness of  $W_{80}Ni_{10}Nb_{10}$  alloy milled for 20 h and sintered at  $1500^{\circ}C$  for 2 h.

### 3.8. Wear study

Figure 9 illustrates the variation of wear depth with sliding distance traversed by the indenter on the sample surface. The sliding distance can be calculated as [18]:

$$\text{Sliding Distance (S.D)} = \left(\frac{R}{60}\right) \times t \times 2\pi r \quad (5)$$

where, R is the number of rotation per minute traversed by the indenter on sample surface, t is time in sec (600 s), r is track radius (4 mm) measured from the center of the sample to the track. It is evident from figure 9 that wear depth increases with increasing load. The results can be attributed to pushing out the intermetallic particles from matrix to the wear track during abrasion which can eventually enhance the wear process. The wear track width also increases with increase in the load as revealed from figure 10. Nuthalapati et al. have reported that three body motion mechanism is responsible for increase in the wear due to increase in abrasion effect at higher load [19].

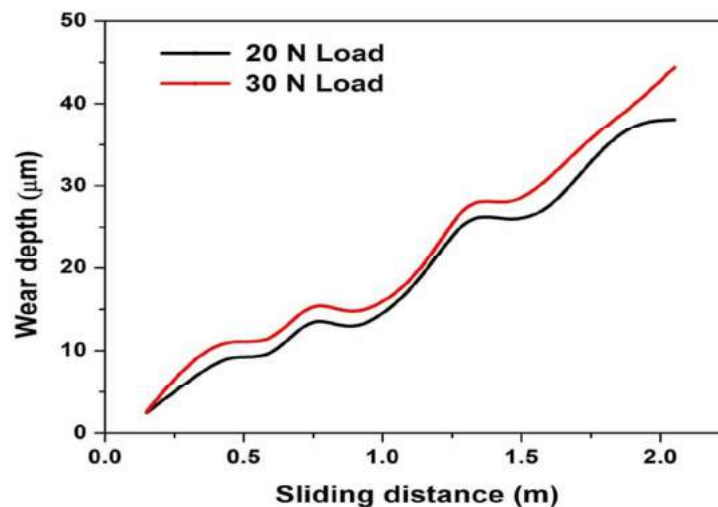


**Figure 9.** Variation of wear depth of  $W_{80}Ni_{10}Nb_{10}$  alloy milled for 20 h and sintered at  $1500^{\circ}C$  for 2h.

Wear rate at maximum wear depth for both 20 N and 30 N load was evaluated by using archard equation [20]. Wear rate is the wear volume per unit load per sliding distance. The measured wear rate at maximum wear depth was recorded  $4.01 (\times 10^{-15}) \text{ m}^3/\text{Nm}$  for 20 N load and  $4.43 (\times 10^{-15}) \text{ m}^3/\text{Nm}$  for 30 N load respectively.

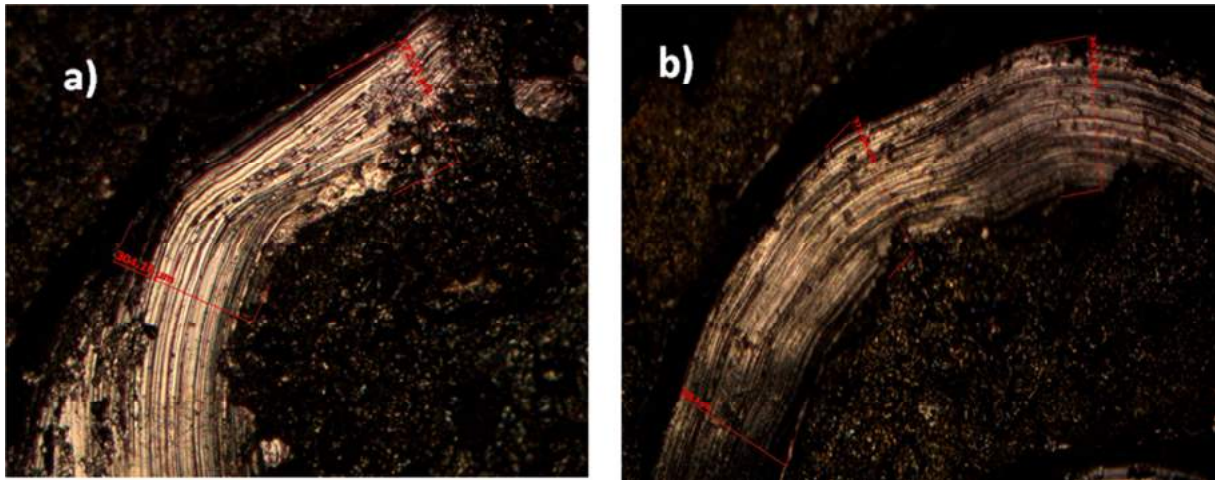


**Figure 10.** Micrograph of wear track at a) 20 N b) 30 N load.

#### 4. Conclusions

From the fabrication, microstructural characterizations and evaluation of mechanical properties of the investigated alloy, the following conclusions can be drawn:

- $\text{W}_{80}\text{Ni}_{10}\text{Nb}_{10}$  alloy powder can be effectively produced by mechanical alloying.
- Crystallite size of tungsten in  $\text{W}_{80}\text{Ni}_{10}\text{Nb}_{10}$  reduces with increasing milling time and minimum crystallite size of 34 nm is achieved at 20 h of milling.
- Expansion of the lattice parameter of tungsten in  $\text{W}_{80}\text{Ni}_{10}\text{Nb}_{10}$  records 0.04% at 10 h and contraction upto 0.02% at 20 h of milling.
- Bright field TEM image and corresponding SAD pattern reveals the presence of nanocrystalline BCC-W phase with 20-30 nm in size at 20 h of milling.
- Presence of NbNi intermetallic is evident in the sintered alloy due to Ni rich liquid phase formation at the selected sintering temperature.
- Microhardness value increases with decrease in load due to smaller indentation and detection error of the diagonals of the indentation at lower loads.
- Wear rate at maximum wear depth increases with increase in load due to enhanced abrasion effect at higher load.

#### References

- [1] Patra A 2012 *Microscopy and Analysis* **26** (5) 14-15.
- [2] Glieter H 2001 *Acta. Mater.* **48** 1.
- [3] Koch C 1997 *Nanostruct. Mater.* **9** 13.
- [4] Suryanarayana C 1998 *Mechanical Alloying* ASM Handbook **7** 80.
- [5] Suryanarayana C 2001 *Prog. Mater. Sci.* **46** 1-184.
- [6] Cullity B 1978 *Elements of X-ray diffraction* **2** (Addison Wesley: Philippines) 86-88.

- [7] Williamson G and Hall W H 1953 *Acta. Mater.* **1** 22.
- [8] Zhao Y H, Sheng H W and Lu K 2001 *Acta. Mater.* **49** 365–375.
- [9] Nuthalapati M, Karak S K, Majumdar J D and Basu A 2014 *Metall. Mater. Trans. A* **45A** 3748-3754.
- [10] Jenkins R and Snyder R L 1996 *Introduction to X-ray Powder Diffractometry* (J Wiley & Sons Inc: New York).
- [11] Chattopadhyay P, Nambissan P M G, Pabi S K and I Manna 2001 *Appl. Surf. Sci.* **182** 308-312.
- [12] Singh V 2002 *Physical Metallurgy* **1** (Standard Publisher Distributor: New Delhi) 63-64.
- [13] Patra A, Karak S K and Pal S 2015 *Proc. Nat. Conf. on Processing and Characterization of Materials (Rourkela)* vol 75 (Bristol: UK/IOP Science) 012032.
- [14] Li X, Cheng Z, Hu K, Chen H and Yang C 2015 *Vacuum* **114** 93-100.
- [15] Ozkan N and Briscoe B J 1994 *J. Eur. Ceram. Soc* **14** 143-151.
- [16] Ayers L J 2012 *The Hardening of Type 316 L Stainless Steel Welds with Thermal Aging* Massachusetts Institute of Technology.
- [17] Dieter G 1928 *Mechanical Metallurgy* SI Metric Edition (McGraw-Hill Co: Singapore) 189-93.
- [18] Patra A, Karak S K and Pal S 2015 *Microscopy and Analysis* **29(4)** 18-22.
- [19] Nuthalapati M, Karak S K and Basu A 2015 *Materials Today: Proceedings* **2** 1109-1117.
- [20] Archard J F 1953 *J. Appl. Phys* **24 (8)** 981-988.